Temperature prediction model for bone drilling based on density distribution and *in vivo* experiments for minimally invasive robotic cochlear implantation

Arne Feldmann[1], Juan Anso[2], Brett Bell[2], Tom Williamson[2], Kate Gavaghan[2], Nicolas Gerber[2], Helene Rohrbach[3], Stefan Weber[2], and Philippe Zysset[1]

[1]Institute for Surgical Technology and Biomechanics

Stauffacherstr. 78, CH-3014, Bern, Switzerland

[2]ARTORG Center for Biomedical Engineering Research

Murtenstr. 50, CH-3010, Bern, Switzerland

[3]Department of Clinical Veterinary Medicine, Vetsuisse Faculty

Länggassstrasse 124, CH-3001, Bern, Switzerland

University of Bern, Switzerland

Contact of corresponding author:

Institute for Surgical Technology and Biomechanics

Tel.: +41 (0)31 631 5928, Fax: +41 (0)31 631 5960

arne.feldmann@istb.unibe.ch

September 1, 2015

Abstract

Surgical robots have been proposed *ex vivo* to drill precise holes in the temporal bone for minimally invasive cochlear implantation. The main risk of the procedure is damage of the facial nerve due to mechanical interaction or due to temperature elevation during the drilling process. To evaluate the thermal risk of the drilling process, a simplified model is proposed which aims to enable an assessment of risk posed to the facial nerve for a given set of constant process parameters for different mastoid bone densities. The model uses the bone density distribution along the drilling trajectory in the mastoid bone to calculate a time dependent heat production function at the tip of the drill bit. Using a time dependent moving point source Green's function, the heat equation can be solved at a certain point in space so that the resulting temperatures can be calculated over time. The model was calibrated and initially verified with *in vivo* temperature data. The data was collected in minimally invasive robotic drilling of 12 holes in four different sheep. The sheep were anesthetized and the temperature elevations were measured with a thermocouple which was inserted in a previously drilled hole next to the planned drilling trajectory. Bone density distributions were extracted from pre-operative CT data by averaging Hounsfield values over the drill bit diameter. Post-operative μCT data was used to verify the drilling accuracy of the trajectories. The comparison of measured and calculated temperatures shows a very good match for both heating and cooling phases. The average prediction error of the maximum temperature was less than 0.7°C and the average root mean square error was approximately 0.5°C. To analyze potential thermal damage, the model was used to calculate temperature profiles and cumulative equivalent minutes at 43°C at a minimal distance to the facial nerve. For the selected drilling parameters, temperature elevation profiles and cumulative equivalent minutes suggest that thermal elevation of this minimally invasive cochlear implantation surgery may pose a risk to the facial nerve, especially in sclerotic or high density mastoid bones. Optimized drilling parameters need to be evaluated and the model could be used for future risk evaluation.

Keywords: Bone drilling, Robotic surgery, Thermal model for bone drilling, In-vivo experimental study, Minimally invasive cochlear implantation, Thermal nerve damage, Cumulative equivalent minutes

1 Introduction

Hearing loss or impairment is a common disability affecting 80 to 100 million people within the European Union alone. Hearing impairment can have an especially large impact on children and often leads to disturbed mental and psychological development [31].

For the treatment of profound to severe hearing loss, a cochlear implant is commonly used to restore a certain level of hearing via direct stimulation of the hair cells. The implantation of the cochlear electrode requires surgical access to the middle ear cavity. This access, which is typically obtained via milling (with a bur) of the lateral skull behind the ear, is in the conventional surgery (mastoidectomy) generally 30-40 times larger than the space required for inserting the electrode. The large access is necessary for the surgeon to visualize and preserve vital anatomical structures embedded in the bone (*e.g.* the facial nerve).

Over the last decades, researchers have aimed to reduce the size of the surgical access in a procedure termed minimally invasive cochlear implantation (MICI). Contrary to the mastoidectomy, the minimal invasive procedure may lead to reduced rates of infection, shorter hospitalization time and improved aesthetic outcomes. The procedure, which involves the drilling of a direct tunnel from the mastoid surface to the middle ear cavity relies on image guidance to ensure structure preservation. Up to date, there is no established minimally invasive procedure, but an image guided surgical robot [7], developed at the university of Bern, has demonstrated sufficient accuracy in *ex vivo* experiments (less than $0.15 \pm 0.08mm$ [6]) to allow precise drilling of the tunnel without damaging close lying anatomy. The narrow arrangement of the sensitive anatomical structures (facial nerve, chorda tympani, ossicles, external auditory canal) means that the planned drilling trajectory may lie as close as 0.5 mm to the facial nerve [30] (see Figure 1).

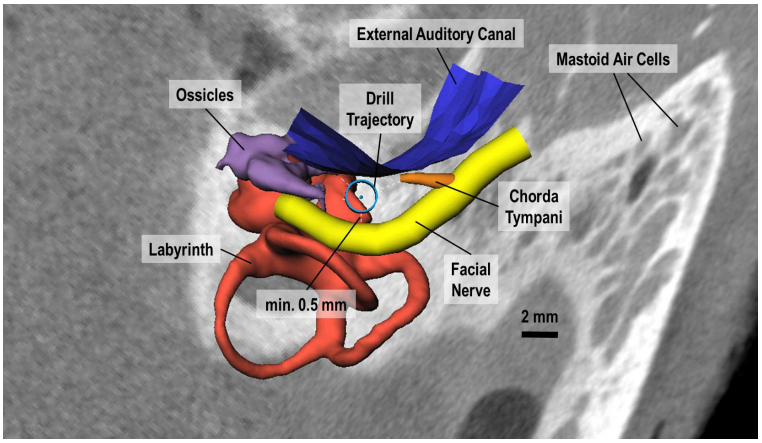

Figure 1: Segmented anatomical structures and drilling trajectory passing through the facial recess. Approximate minimal distance of 0.5 mm between drilling trajectory and facial nerve indicated.

The main risk of minimally invasive cochlear implantation is damage to the facial nerve due to direct contact of the drill bit or due to the temperature elevation generated by the drilling process. The risk of harming the facial nerve due to temperature elevation has been reported in various investigations [19] [2]. The group of Labadie *et al.* reported in an initial clinical trial of minimally invasive cochlear implantation, using template based image guidance, facial nerve damage (palsy) in 1 out of 7 cases and they concluded that it was caused most likely by heat [21]. In conventional cochlea implant surgery, the complication rate of facial nerve palsy (18-19 hours postoperatively) is 0.71% [15].
Little is known, however, about the *in vivo* temperature elevation of surrounding structures experienced due to the drilling process. Several *ex vivo* experiments measuring temperature elevation in cortical bone with different drill bit designs, rotational speeds, feed rates, irrigation types, etc. have been reported [23][4] [5], but varying experimental conditions make comparisons among studies difficult. Whilst it is generally believed that a low rotational speed (around 1000 RPM) and a high feed rate (up to 1 mm/s) leads to a lower overall temperature elevation [23] [3]. The reason for the beneficial lower rotation speed is the reduction of friction. The higher feed rate (in combination with a low rotational speed) leads admittedly to higher cutting forces, but more importantly it decrease the time of heat transfer into the bone. The connected and adverse effects of process parameters need further investigation and optimal process parameters for heat reduction while drilling in the temporal bone are yet to be determined.
The definition of a single set of safe drilling parameters in terms of heat production is complicated by the varying density of the mastoid bone among the population. The mastoid section of the temporal bone is generally pneumatized and thus contains cells of varying size which result in significant dif-

ferences in drilling forces [35]. At the upper and front part of the mastoid process, cells are generally large and irregular and contain air, while in lower parts, their size is generally diminished. Cells at the apex of the process are frequently small and contain marrow. The mastoid can also experience different levels of pneumatisation. In 36.8% of the population the mastoid is completely pneumatized, in 43.2% it is partially pneumatized and in 20% the mastoid is completely dipolic or sclerotic in which case the mastoid bone is solid [18].

A model of temperature elevation relative to cutting force would enable a set of drilling parameters to be assessed for the full range of mastoid density distributions. The modeling of drilling forces and resulting temperatures has, however, been a longstanding problem due to the complex interaction of the cutting tool with the material. To date, there is no satisfactory analytical model which can accurately describe the interaction of cutting tool and working material [1] and the majority of work towards this end has focused on the cutting of metal whereas bone is a brittle and anisotropic material which fails in a damage accumulating process [33].

Force and thermal models for bone drilling have been previously based on calibration experiments [22] or on metal cutting assumptions [26] [24]. There has been recent efforts to model the drilling process in bone with finite element models with promising results for small depths which still require a long computational time[25]. To the knowledge of the authors, a temperature model which accounts for differing forces resulting from varying bone density distributions, that could be used to assess the temperature elevation experienced during drilling into the mastoid, is yet to be described.

Within this work, the effect of bone density on the temperature elevation around the drilling site is evaluated experimentally in an *in vivo* study on sheep. Additionally, the proposed simplified model aims to enable an assessment of risk posed to the facial nerve for a given set of constant process parameters for different mastoid bone densities for minimally invasive cochlear implantation.

2 Materials and Methods

An image guided surgical robot, which was developed for minimally invasive cochlear implantation, was used to allow measurements to be obtained from planned known distances from the drilling site. Contrary to conventional manual drilling, the use of a robotic system also allowed drilling parameters to be controlled during the study. To enable prediction of heat elevation for varying bone density

values, the experimentally measured temperature profiles were also used to calibrate and verify the simplified temperature prediction model. The model is then used for a first judgment of potential thermal damage to the facial nerve using the current process parameters of the minimally invasive robotic cochlear implantation surgery.

2.1 Temperature Prediction Model

Due to difficulties in the analytical modelling of temperature elevation during drilling and the unknown relationship between forces and heat production, a temperature prediction model was developed. It was hypothesized that the temperature elevation is dependent on drilling forces which mechanically depend on the bone density. Therefore a higher temperature is expected for drilling in cortical than in cancellous bone. The force is dependent on drill bit design and process parameters and its bone density dependence has been previously used for on-line verification of the correct drilling path [35]. An analytical model was chosen to model a bone density dependent energy function of the drill bit while the bone material itself is modeled homogeneously. This was done because no material properties are available for the thermal conductivity of different bone densities. The advantage of the analytical model in comparison to a finite element model is that it is simpler, faster and needs minimal computational resources. The consistency of the results supports this choice a posteriori. For the proposed analytical model, it is necessary that only one input parameter is varying (bone density) while all the other parameters of the system (*e.g.* rotational speed, feed rate, irrigation, CT machine, etc.) remain constant.

The density distributions D(x) along the different drilling trajectories are extracted from the CT-images by averaging the Hounsfield grey values (HU) in a circle with the diameter of the drill bit for every layer of CT-images perpendicular to the drilling direction in steps of 0.15 mm. HU-values are not physical units and are calibrated for each individual CT machine. Therefore, the relationship between forces and densities may vary and can only be compared for the same machine. In general a HU value of 0 is water, a value of 300-700 HU represents cancellous bone and value of $\geqslant$ 1200 or higher for compact bone [27]. Values higher than 2000 HU are likely from the petrous part of the bone which is the densest bone in the body [13]. A quantitative comparable measurement could be accomplished using a calibration phantom.

Using the constant velocity of the drill bit, v (feed rate in $[\frac{m}{s}]$), the density distribution D(x) of a

drilled trajectory can be expressed as a function of time, D(t). The relationship between force and bone density can then be represented by the equation

$$F(t) \sim D(t)^b \tag{1}$$

in [N]. This power relationship was chosen, because it represents the power dependence of strength and stiffness of porous bone with respect to structural density [9]. The calibration coefficient "b" in equation 1 describes this relationship. A second calibration constant "A" is incorporated which describes the influence of the CT-machine and all fixed parameters of the drilling process (e.g. rotational speed, feed rate, drill bit). It also describes the fraction of energy which is turned into heat. The equation for the time dependent thermal energy (heat rate in [Watt]) produced by the drill bit per unit time, can then be expressed as:

$$\dot{Q}(t) = v \cdot A \cdot D(t)^b \tag{2}$$

$\dot{Q}(t)$ is set to 0 for all negative HU values and at the end of the drilling process because the drill bit is extracted.

The drill bit is modeled as a moving point source in a 3-dimensional space for calculating the temperature elevation over time. In general, the non steady-state heat conduction equation is given by:

$$\frac{\partial T}{\partial t} = \alpha \left(\frac{\partial^2 T}{\partial x^2} + \frac{\partial^2 T}{\partial y^2} + \frac{\partial^2 T}{\partial z^2} \right) \tag{3}$$

With dT as temperature rise and the thermal diffusivity α for an infinite body. This equation can be solved with a Green's function for an instantaneous point source (dQ) located at x_0, y_0, z_0 and evaluated at a point x, y, z for time t [8]:

$$dT(t, x, y, z) = \frac{dQ}{8\rho c_p (\pi \alpha t)^{\frac{3}{2}}} \, e^{-\frac{(x-x_0)^2+(y-y_0)^2+(z-z_0)^2}{4\alpha t}} \tag{4}$$

With the constant thermal diffusivity $\alpha = \frac{k}{\rho c_p}$ in $[\frac{m^2}{s}]$, where k is the thermal conductivity, ρ the density and c_p the specific heat. For calculating the temperature elevations in the temporal bone, **homogeneous** material constants from compact bone were used: $k = 0.55 \frac{W}{mK}$ [11]; $\rho = 1800 \frac{kg}{m^3}$;

$c_p = 1260 \frac{J}{kgK}$ [10]. Due to the low homogeneous thermal conductivity of bone and therefore confined space of temperature elevation deep inside the head with constant body temperature, infinite boundary conditions were used.

In the case of a drill bit advancing into bone, the point source is continuous, varying in time and moving along the x-axis with velocity v in$[\frac{m}{s}]$ (see Figure 2). So that the equation can be modified and integrated over time:

$$T(t,x,y,z) = T_0 + \int_0^t \frac{\dot{Q}(\tau)}{8\rho c_p(\pi\alpha\tau)^{\frac{3}{2}}}\, e^{-\frac{(x-x_0-vt)^2+(y-y_0)^2+(z-z_0)^2}{4\alpha\tau}}\, d\tau \tag{5}$$

With $\dot{Q}(\tau)$ as the time dependent energy function from equation 2 and T_0 as the initial body temperature. A similar formulation has been used for modeling a laser drilling process [28].

The coordinates x_0, y_0, z_0 describe the initial position of the point source which resembles the starting point of the drilling at the outer skull surface. The coordinates x, y, z describe the position where the temperatures are evaluated (measured).

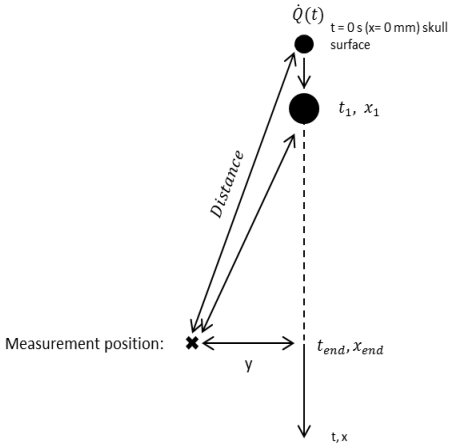

Figure 2: Simplification of the point source moving along the x-axis. The velocity of the moving point is equal to the feed rate of the drilling process.

A program was written (Matlab with symbolic toolbox, Mathworks, USA) to solve the integral over time. The integral is evaluated longer in order to describe the cooling phases as well. The integral superimposes the temperatures at each time step which leads to characteristic temperature curves.

2.2 *In vivo* Experiments

To investigate variance in temperature elevation experienced during direct minimally invasive robotic cochlear access drilling for a set of current standard drilling parameters, an *in vivo* study was conducted. The overall setup is similar to the planned future clinical application. An image guided robotic system designed for the drilling of a minimally invasive access to the cochlea [7] was used to drill cylindrical holes with controlled drilling parameters in a pre-operatively planned location.
Experiments were performed on four sheep, prepared at the veterinary hospital of the University of Bern. The trial was approved by the committee for animal experiments of the canton of Bern, Switzerland (BE 56/12). The sheep temporal bone anatomy is generally very similar to the human anatomy and is regularly used as a study model in ear surgery [32]. Four bone screws were inserted into the temporal bone to enable intraoperative image registration. Afterwards the sheep were transferred to a CT machine where the images (0.2x0.2x0.4 mm) were acquired (Philips Brilliance 16p, Philips, Netherlands). Based on these images, the robotic system's planning software was used to plan drilling trajectories in the temporal bone for each sheep [16]. For the drilling procedure itself each sheep was positioned in sternal recumbency on an OR-table and the head was fixed with an invasive pin-type head clamp (Figure 3). During the procedure, a veterinary doctor performed standard measures to maintain all vital parameters of the sheep in a normal physiological range.

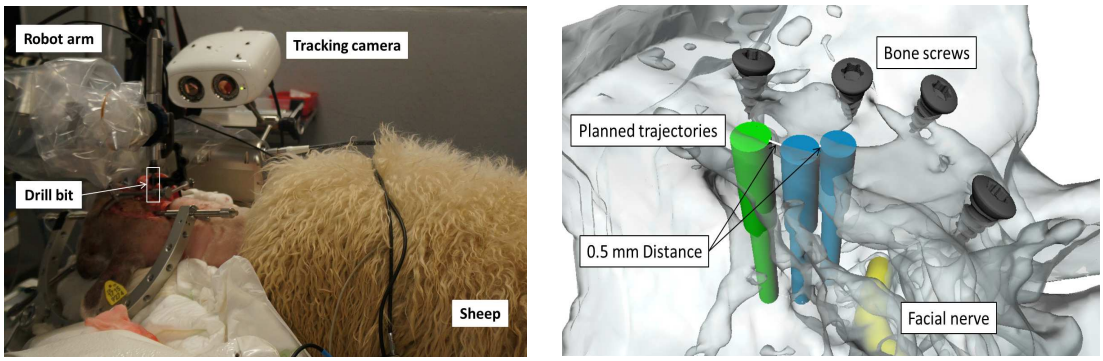

Figure 3: Left: *In vivo* experimental setup with surgical robot (temperature measurement equipment not visible); Right: Example of 3 planned drilling trajectories with a distance of 0.5 mm in-between the edges. All 12 holes are planned accordingly. Drilled holes function in many cases as measurement hole for the next drilling. In this case is the green trajectory is the first measurement hole for the first drilling trajectory (closer blue trajectory).

The robot and the optical tracking camera were mounted onto the OR-table and the positions of the screws were determined with an optically tracked registration tool [16]. The drill bit is a spiral tungsten carbide step drill bit (Louis Belet, Switzerland) with two diameters (⌀ 1.8 mm x 10 mm , ⌀

2.5 mm x 20 mm). The two step design and hard material increases stiffness whilst providing greater lateral distance to the facial nerve. A similar drill bit has been proven most accurate for temporal bone drilling [20]. Four to six trajectories were drilled into each sheep for temperature measurement with a rotational speed of 5000 RPM (due to limitation of the motor to drill with 1000 RPM) and an average feed rate of 0.2 mm/s. A configuration error in the settings of the robotic system resulted in a velocity of 0.3 mm/s in the fourth sheep.

A custom made temperature measurement device (Fig. 4) was fabricated. The probe was designed to fit into the drilled tunnels and to measure temperatures at its tip. For measuring the temperatures, a thermocouple (Typ T, Omega Engineering, USA) was built into the tip of the custom made device and connected to a recording unit (RDXL4SD, Omega Engineering, USA). Drilling trajectories of approximately 15-20 mm long were planned 0.5 mm from each other. Depths of measurement holes were in some cases planned slightly different in order to avoid ending in a cavity, but correct values were later used as input parameter for the model. During the drilling of a trajectory, the temperature measurement probe was inserted into the previously drilled neighboring hole. A small amount of thermal paste was used and proper bone contact was ensured by pressing the probe into the hole. Due to the geometry of the drill bit (Fig. 4), the planned distance between the thermocouple at the tip and the center of the drilled hole was exactly 3 mm which is used for the y-value in eq. (5). Whereas the x-value in this equation corresponds to the depth of the measurement hole.

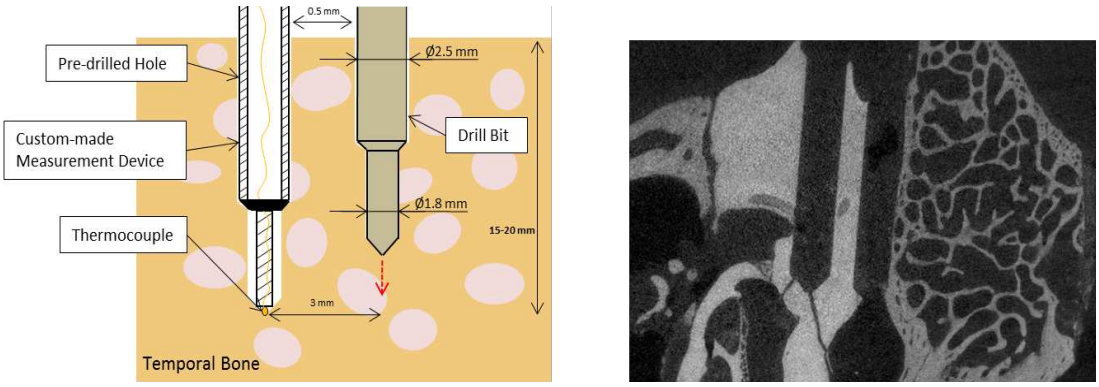

Figure 4: Left: Measurement setup with thermocouple and drill bit advancing into the bone; Right: Post-op μCT of two neighboring drilled holes.

Temperature data was recorded with a frequency of 1 Hz for the heating and cooling (after extraction of drill bit) period until the temperature value decreased to initial body temperature ($\approx 36.7°C$). Measurements were excluded if a blood vessel was hit. The sheep were sacrificed after the surgery

and the temporal bone samples were extracted. Post operative μCT images (Scanco μCT 40, Scanco, Switzerland) were taken with a resolution of 18 μm (Fig. 4).

The measured data was then used for calibrating the two constants and verifying the calculated temperature profiles. For the calibration procedure, initial trial constants for A, b were chosen. These estimated constants were then calibrated using all measurement data in order to find the universal best fit. This was accomplished by applying an iterative fitting to minimize both the mean root square error (RMSE) and the temperature prediction error at maximum temperature (ERMT) for the measured and the calculated temperatures. The combination of both parameters which gave the best results was then used for further evaluation.

After comparing the measured and calculated temperature profiles, the model was also used to calculate temperatures at a distance closer to the drilling trajectory which may resemble the actual minimal nerve position for MICI surgeries.

3 Results

3.1 Temperature Prediction Model

Within this experiment, a large variety of bone density distributions were encountered, which allows a calibration of the two constants. They were evaluated as $A = 2.11 * 10^{-4}$ and $b = 1.815$. The accuracy of the drilled holes was verified using the post-op μCT images to be 0.19 mm with a standard error of 0.05 mm.

Figure 5 shows the linear regression between calculated and measured maximal temperatures. An adjusted $R^2 = 0.9566$ was calculated. In the two cases where higher temperatures were measured, the model prediction is still reasonably accurate. A calibration of the model without these two measurements ($A = 1.21 * 10^{-4}$, $b = 1.89$) altered the regression parameters and the adjusted R^2 only slightly ($R^2 = 0.9579, y = 0.93954 \cdot x + 2.11612$).

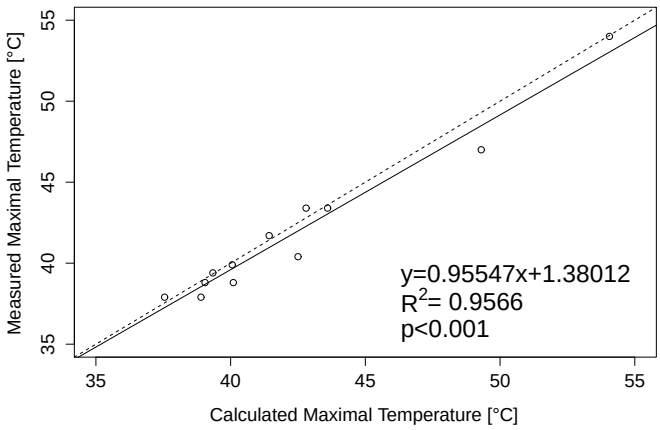

Figure 5: Regression between calculated and measured maximal temperatures with calibration of the model using all measurement data. Linear regression line and y=x line (dashed) are shown.

In Figure 6, the measured and calculated temperatures over the measured time period are depicted along with the bone density profile (D(t) expressed in Hounsfield units) for each drilled trajectory. The rise of the density profile shows the start of the drilling process, while the drop of the density profiles to 0 HU denotes the end of the drilling process. All negative HU values were set to zero. The blue point shows at which depth (time) the drilled trajectory reaches (would reach) the depth of the measurement hole. Temperature and density profiles were determined relative to time using the known constant feed rate of the drilling process. The RMSE and ERMT, which describe how well the calculated and measured temperature profile curves correlate, are also shown in each graph.
The dependence of temperature on bone density elevation is clearly visible. Temperature elevation is significantly higher when drilling in cortical than cancellous bone. For the maximum temperature elevation, the density value at the end of each drilling trajectory is most important. Due to the low thermal conductivity of bone, the temperature drop within millimeters is significant, so that the temperature is governed by the density values which are closest to the measurement position (last millimeters of drilling depth). The highest measured temperatures of sheep 3, trajectory 1 and sheep 4, trajectory 2 are due to the very high density at the end and the nearly same depth of measurement and drilling hole.

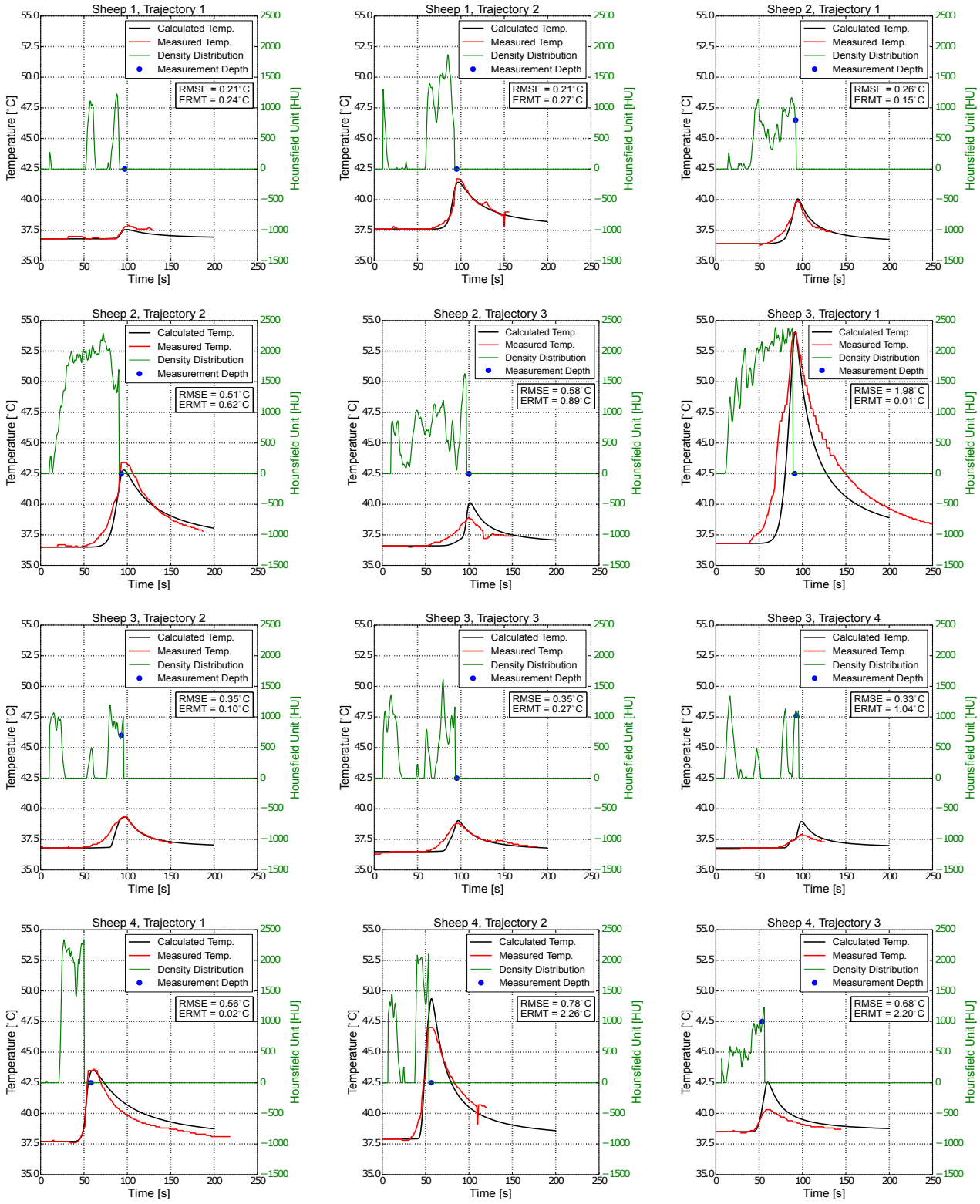

Figure 6: Comparison of calculated and measured temperatures over time for a distance of 3 mm. Root meant square errors (RMSE) and errors at maximal temperature (ERMT) of measured and predicted temperatures are shown. The green line shows the density profile of the drilling trajectory. The rise of the density profile above 0 HU denotes the start of the drilling process, while the drop to 0 HU shows the end of the drilled trajectory. All negative HU values were set to zero. The blue point shows at which depth (time) the drilled trajectory reaches (would reach) the depth of the measurement hole.

3.2 Thermal Nerve Damage

Temperatures were measured at a distance of 3 mm which results from the step design of the drill bit. The facial nerve however might be as close as 0.5 mm to the edge of the drilled tunnel. For this the y_0-coordinate of the measurement point in formula (5) is set to 1.4 mm which results in the distance of 0.5 mm to the edge of the drilled hole (Fig. 1).

The extent of thermal damage of biological tissues depends on the sensitivity of the tissue, the temperature elevation and on the exposure time. To evaluate the tissue damage, the cumulative equivalent minutes at 43°C (CEM43°C) were used to relate time and temperature elevation [29]. Each tissue or cell has a different threshold which rises exponentially with higher temperatures.

The CEM43°C value, mostly used for describing hypertermia in MR saftey or RF-heating treatment, can be calculated as [29]:

$$CEM43°C = \int_0^{t=t_{final}} R(T)^{43-T(t)} dt \quad with \quad R(T) = \begin{cases} 0.5, & \text{if } T > 43°C \\ 0.25, & \text{otherwise} \end{cases} \tag{6}$$

In general, it is a comparison method of the area under the time-temperature curve. The maximum temperature and the CEM43°C are shown in the graphs. The y-scale in Figure 7 is now changed to 100°C.

Due to the low thermal conductivity of bone, it is clearly visible that there is a big difference in temperatures for a difference in distance of just 1.6 mm. The higher temperature drop for higher measured temperatures and the flattening of the curve at a larger distance corresponds to that. It also empathize the fact that damage to the facial nerve has to be evaluated for a worst case scenario for the closest possible distance.

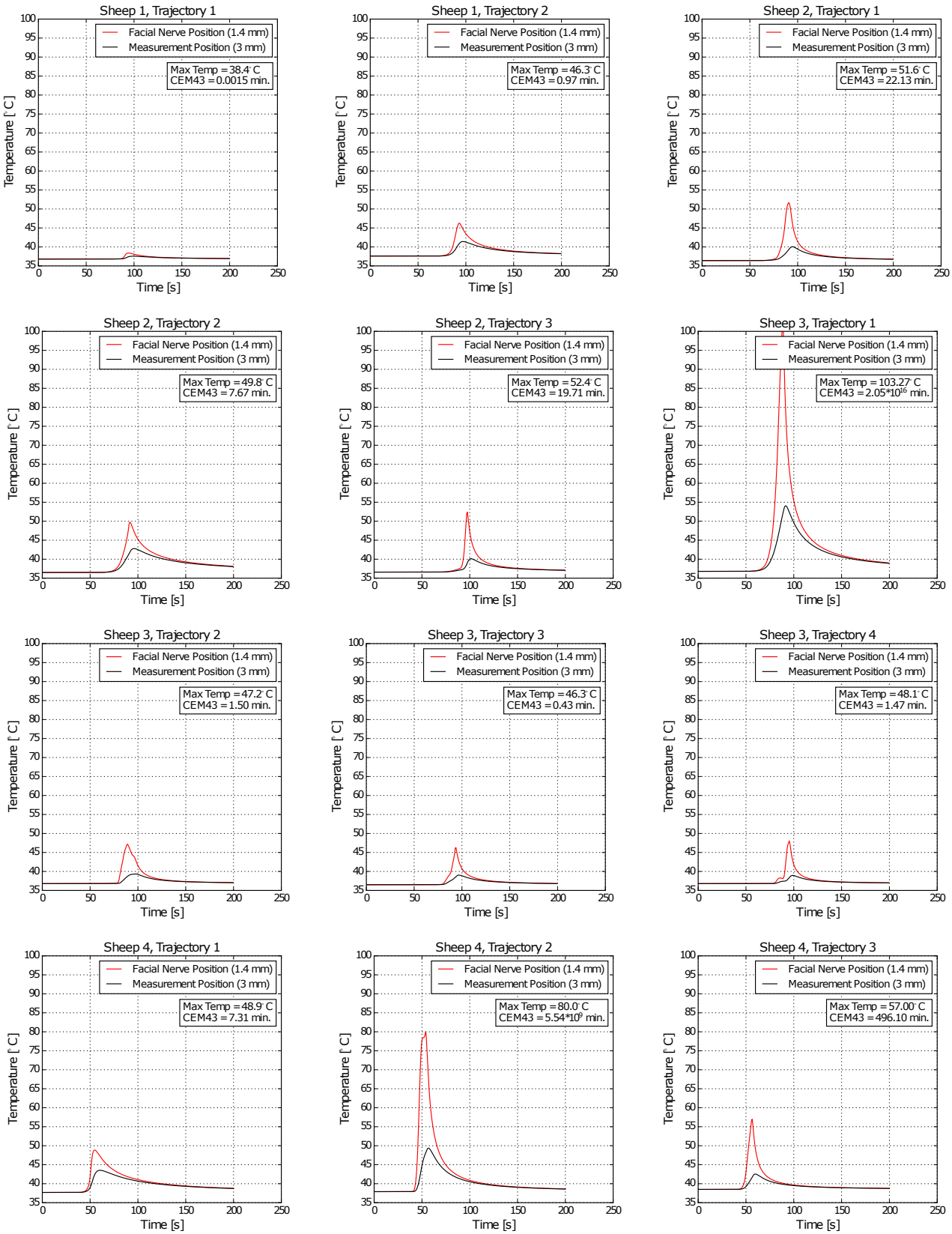

Figure 7: Calculated temperature curves for measurement position and theoretical minimum distance to facial nerve (1.4 mm distance to axis represents distance of 0.5 mm to the edge of the drilled hole). Maximal reached temperatures and cumulative equivalent minutes at 43°C are shown.

4 Discussion

Within this work, the effect of bone density distribution on temperature change in the mastoid bone during direct drilling to the cochlea and its possible effect on the facial nerve have been investigated. Additionally, a temperature change prediction model for a specific set of drilling parameters has been proposed and initially evaluated against *in vivo* measurements. The model, which allows patient specific temperature prediction based on bone density distributions, has enabled temperature change predictions at a distance from the drill site relevant for direct cochlear access drilling. The advantage of the model compared to other previously described models for bone drilling temperature calculation is that it is very simple. Once calibrated, temperatures can be calculated within seconds. It could be most useful for robotic surgery in which many of the drilling process parameters can be kept constant. Drilling forces also do not need to be evaluated because density dependent temperature profiles are calibrated directly. If the model can be calibrated more easily and proves to be reliable, it could be used for risk assessment during robotic surgery.

Whilst further verification and validation is required, the large range of bone densities encountered in the experiment allowed a calibration and initial verification of the proposed model. The model does however, incorporate certain deficiencies which may reduce the accuracy of the predicted temperatures. By modeling the drill bit as a point with a concentrated heat flux with no lumped heat capacity, prediction errors at the boundaries of the drill bit may occur. In the future, the model could be enhanced by representing the drill, for example, as a ring source.

Additionally the thermal conductivity of cancellous and pneumatized bone is currently unknown, so that a homogeneous conductivity value of cortical bone was used. Replacing this value with one more representative of the variations of the mastoid bone or with a patient specific approximation could further improve accuracy of the prediction model. Finally, the sensitivity of the model to the exact process parameters and CT machine calibration is unknown and should be evaluated in future work. When compared, the calculated and measured temperature curves (Fig. 6) show an overall good match. The calculated temperatures closely resemble the characteristic heating and cooling curves of a low conductive material and show similar results to those previously reported in the literature [23]. The mean root square error for all cases was 0.56°C and the mean error of the average maximum temperature was 0.67°C. The model is also able to predict the higher temperatures (up to 55°C) if

it is calibrated using only the low temperature range ($< 45°C$) as mentioned in the result section. The larger error of the temperature prediction experienced in sheep 4 was most likely due to the mentioned deviation in feed rate and highlights the dependency on drilling parameters. The model is based on the assumption that all drilling parameters are kept constant. It has been reported that a higher feed rate leads to a lower overall temperature due to the shorter time exposure [23]. If the model is calibrated with only data from sheep 1-3 the mean RMSE error reduces to 0.52°C and the mean ERMT value reduces to 0.39°C for sheep 1, 2 and 3.

The large variations in temperature profiles presented in Figure 6 demonstrate the strong dependency of temperature on bone density. The model is sensitive enough to describe the large contribution of temperature rise resulting from the density closest to the measurement position. This can be seen by comparing temperature profiles of trajectory 2 of sheep 2 with trajectory 1 of sheep 3 in Figure 6. The density profiles are very similar except that the density drops to around 1500 HU for trajectory 2 of sheep 2 for the last millimeters of drilling which results in a lower maximum temperature.

In future work the exact relationship between bone density and drilling forces and temperature will be investigated and possibly a constant can be found which defines this relationship. The determined value of $b = 1.815$ is interestingly very close to the general relationship for stiffness of cancellous bone ($b = 1.6..1.8$) [17]. It is a good indication that the relationship for bone density and drilling force might correlate with stiffness of different bone densities. In this case, just one parameter has to be calibrated.

The use of a surgical robot in the presented experiment allowed *in vivo* temperature measurements at highly controlled drilling conditions to be performed at the depth of the facial nerve. The errors in temperature profile calculations may also be impacted by inaccuracies in temperature measurements due to experimental conditions. Even though the custom made thermocouple device was designed to ensure good contact of the bone, the lack of contact (e.g. due to small cavities) is a potential source of error. Additionally a small unnoticed blood flow within the bone could conduct heat away due to convection. To the authors knowledge, few *in vivo* studies for bone drilling and none measuring temperatures at such a drilling depth, have been previously reported.

The possible effect of temperature on the facial nerve during direct cochlear access drilling has been previously proposed and experienced in a clinical study [21], but this work presents the first reported quantified data that can be used to evaluate the effect of the approach on temperature rise and

possible structure damage. Due to the low thermal conductivity of bone, heat accumulates in a small region and is not conducted away. This can lead to a small necrotic zone around the drill hole in a region in which the facial nerve may lie. Thermal nerve damage cannot be evaluated by looking at the maximal temperatures alone. Within this work, possible nerve damage has been determined using the CEM43°C value which incorporates both time and temperature elevation. The CEM43°C at the clinically relevant 0.5 mm from the edge of the drill bit was calculated from the predicted temperature profiles presented in Figure 7. The previous results suggest that a fair prediction of temperature is possible for a closer distance to the drilling trajectory. The earlier and higher maxima of the predicted temperatures (Figure 7) are reasonable and the large temperature drop for different distances to the drilled hole is consistent with the literature for bone drilling [23]. Further verification of the predicted profiles for a closer distance will however be performed in future studies by using a drill bit with a constant diameter.

Determining the rate of possible damage to the facial nerve based on the CEM43°C or any other measure of thermal exposure is difficult as no single accepted threshold for thermal nerve damage exists. Using the threshold of 44°C for 30 min (CEM43°C = 60 min) determined by Haveman *et al.* [19] who reviewed the effects of hyperthermia on the peripheral nervous system, 3 of the drilled trajectories (Sheep 3/Trajectory 1, S4/T3+T4) would have resulted in permanent nerve damage. De Vrind *et al.* [34] suggested that a threshold for temporary nerve damage might even be lower. He also found that increasing the temperature by 1°C decreases the allowed heating time by 50%. All these studies focus on long heating time with lower temperatures. This is why the threshold of bone necrosis [14] (47°C for 1 min $\rightarrow$ CEM43°C = 16 min), which is commonly used in bone drilling research, could be used for further assessment. At this temperature and time around 80% of the osteocytes become either apoptotic or necrotic [12]. When applied, 5 drilled trajectories (S2/T1+T3, S3/T1, S4/T2+T3) would violate this threshold.

Before a more definite prediction of nerve damage can be made, histological data obtained after thermal exposure in a controlled setting is required. Such data will be collected in future experiments. Whilst the possible rate of damage to the facial nerve during direct cochlea access drilling is still unknown, it is evident from these results that thermal nerve damage could be an issue, especially for persons with a sclerotic mastoid. Drilling protocols should be designed to reduce the risk of thermal damage and the use of a model such as the one presented herein could help to evaluate the safety of

the procedure preoperatively, based on patient CT data.

In future studies, drilling parameters (*e.g.* rotational speed and feed rate) need to be found which ensure a safe drilling process for all possible bone density distributions. The drilling protocol could include a strategy for cooling with a constant automatized rate of irrigation in combination with a pecking movement of the drill bit (drilling in intervals) to improve chip evacuation.

Additionally, when more material parameters are available, a more detailed finite element model could be developed to compare it to the suggested model.

4.1 Conclusion

A simple temperature prediction model that is based on bone density distribution was proposed and successfully evaluated against *in vivo* experiments. The results suggest that minimally invasive cochlear implantation surgery with current process parameters may pose a risk to the facial nerve, especially in sclerotic or high density mastoid bones. Safe drilling parameters need to be found and evaluated. For minimally invasive cochlear implantation, the temperature prediction model may be particularly useful for assessing risk to the facial nerve on a patient specific basis during the planning phase of the procedure. For this, validation of the model using human temporal bone is necessary and its robustness and accuracy needs to be evaluated in a controlled setup.

5 Acknowledgments

The authors wish to thank Christina Precht from the Vetsuisse Department for her help in conducting the *in vivo* sheep studies. The authors would also like to thank Nano Tera and the Swiss National Science Foundation for funding the research within the hear restore project (RTD 2013).

6 References

References

[1] Arrazola, P., T. Özel, D. Umbrello, M. Davies, and I. Jawahir; Recent advances in modelling of metal machining processes; CIRP Annals - Manufacturing Technology; 62:695–718; 2013.

[2] Aslan, A., H. S. Vatansever, G. G. Aslan, G. Eskiizmir, and G. Giray; Effect of thermal energy produced by drilling on the facial nerve : histopathologic evaluation in guinea pigs; The Journal of Laryngology & Otology; 119:600–605; 2005.

[3] Augustin, G., S. Davila, K. Mihoci, T. Udiljak, D. S. Vedrina, and A. Antabak; Thermal osteonecrosis and bone drilling parameters revisited.; Archives of orthopaedic and trauma surgery; 128:71–7; 2008.

[4] Augustin, G., S. Davila, T. Udilljak, T. Staroveški, D. Brezak, and S. Babić; Temperature changes during cortical bone drilling with a newly designed step drill and an interally cooled drill; International Orthopadics; 36:1449–1456; 2012.

[5] Augustin, G., T. Zigman, S. Davila, T. Udilljak, T. Staroveski, D. Brezak, and S. Babic; Cortical bone drilling and thermal osteonecrosis; Clinical biomechanics (Bristol, Avon); 27:313–25; 2012.

[6] Bell, B., N. Gerber, T. Williamson, K. Gavaghan, W. Wimmer, M. Caversaccio, and S. Weber; In Vitro Accuracy Evaluation of Image-Guided Robot System for Direct Cochlear Access; Otology and Neurotology; 34:1284–1290; 2013.

[7] Bell, B., C. Stieger, N. Gerber, M. Caversaccio, and S. Weber; A self-developed and constructer robot for minimally invasive cochlear implantation; Acta oto-laryngologica; 132:355–360; 2012.

[8] Carslaw, H. and J. Jeager; Conduction of Heat in Solids; Oxford University Press, Oxford, 1986; 2 edition edition.

[9] Carter, D. and W. Hayes; The compressive behavior of bone as a two-phase porous structure; Journal of Bone and Joint Surgery; 59:954–962; 1977.

[10] Chen, H. L. and A. A. Gundjian; Specific heat of bone; Medical & Biological Engineering; 1974–1976; 1974.

[11] Davidson, S. R. and D. F. James; Measurement of thermal conductivity of bovine cortical bone; Medical engineering & physics; 22:741–7; 2000.

[12] Dolan, E. B., M. G. Haugh, M. C. Voisin, and D. Tallon; Thermally Induced Osteocyte Damage Initiates a Remodelling Signaling Cascade; Plos One; 10:1–17; 2015.

[13] Drake, R. L., A. W. Vogl, and A. W. Mitchel; Gray's Anatomy; Churchill Livingstone, Philadelphia, 2014; 3 edition edition.

[14] Eriksson, R. and T. Albrektsson; The Effect of heat on bone regeneration: An experimental study in the rabbit using the bone growth chamber; Journal of Oral and Maxillofacial Surgery; 42:705–711; 1984.

[15] Fayad, J. N., G. B. Wanna, J. N. Micheletto, and S. C. Parisier; Facial Nerve Paralysis Following Cochlear Implant Surgery; The Laryngoscope; 113:1344–1346; 2003.

[16] Gerber, N., B. Bell, K. Gavaghan, C. Weisstanner, and M. Caversaccio; Surgical planning tool for robotically assisted hearing aid implantation; International Journal CARS; 9:11–20; 2014.

[17] Gross, T., D. H. Pahr, and P. K. Zysset; Morphology – elasticity relationships using decreasing fabric information of human trabecular bone from three major anatomical locations; Biomech Model Mechanobiol; 12:793–800; 2013.

[18] Gulya, A. J. and H. Schuknecht; Anatomy of the termporal bone with surgical implications; informa healthcare, Washington, 2007; 3 edition edition.

[19] Havemann, J. van der Zee, J. Wondergems, J.; Effects of Hypertermia on the peripheral nervous system: a review; International Journal of Hyperthermia; 20:371–391; 2004.

[20] Kobler, J.-P., M. Schoppe, G. J. Lexow, T. S. Rau, O. Majdani, L. a. Kahrs, and T. Ortmaier; Temporal bone borehole accuracy for cochlear implantation influenced by drilling strategy: an in vitro study.; International journal of computer assisted radiology and surgery; 2014.

[21] Labadie, R. F., R. Balachandran, J. H. Noble, G. S. Blachon, J. E. Mitchell, F. a. Reda, B. M. Dawant, and J. M. Fitzpatrick; Minimally invasive image-guided cochlear implantation surgery: First report of clinical implementation; The Laryngoscope; 1–8; 2013.

[22] Lee, J., B. A. Gozen, and O. B. Ozdoganlar; Modeling and experimentation of bone drilling forces; Journal of biomechanics; 45:1076–83; 2011.

[23] Lee, J., O. B. Ozdoganlar, and Y. Rabin; An experimental investigation on thermal exposure during bone drilling; Medical engineering & physics; 34:1510–20; 2012.

[24] Lee, J., Y. Rabin, and O. B. Ozdoganlar; A new thermal model for bone drilling with applications to orthopaedic surgery; Medical engineering & physics; 33:1234–44; 2011.

[25] Lughmani, W. a., K. Bouazza-Marouf, and I. Ashcroft; Finite element modeling and experimentation of bone drilling forces; Journal of Physics: Conference Series; 451:012034; 2013.

[26] Maani, N., K. Farhang, and M. Hodaei; A Model for the Prediction of Thermal Response of Bone in Surgical Drilling; Journal of Thermal Science and Engineering Applications; 6:041005; 2014.

[27] Misch, C. E.; Contemporary Implant Dentistry; Mosby, Elsevier, St. Louis, 2007; 3 edition edition.

[28] Paek, U. and F. Gagliano; Thermal Analysis of Laser Drilling Process; IEEE Journal of Quantum Electronics; 8:112–119; 1972.

[29] Sapareto, S. A. and W. C. Dewey; Thermal dose determination in cancer therapy; International Journal of Radiation Oncology, Biology, Physics; 10:787–800; 1984.

[30] Schipper, J., A. Aschendorff, and R. Laszig; Navigation as a quality management tool in cochlear implant surgery; J Laryngol Otol; 118:764–760; 2004.

[31] Shield, B.; Evaluation of the social and economic costs of hearing impairment. A report for Hear-it; Technical Report October; 2012.

[32] Soares, H. B. and L. Lavinsky; Histology of sheep temporal bone.; Brazilian journal of otorhinolaryngology; 77:285–292; 2011.

[33] Sugita, N. and M. Mitsuishi; Specifications for machining the bovine cortical bone in relation to its microstructure; Journal of biomechanics; 42:2826–9; 2009.

[34] de Vrind, H. H., J. Wondergem, and H. de Vrind; Hyperthermia-induced damage to rat sciatic nerve assessed in vivo with functional methods and with electrophysiology; Journal of Neuroscience Methods; 45:165–174; 1992.

[35] Williamson, T. M., B. J. Bell, N. Gerber, L. Salas, P. Zysset, M. Caversaccio, and S. Weber; Estimation of tool pose based on force-density correlation during robotic drilling.; IEEE transactions on bio-medical engineering; 60:969–76; 2013.

7 Tables, figure legends

Figure 1: Segmented anatomical structures and drilling trajectory passing through the facial recess. Minimum distance of 0.5 mm between drilling trajectory and facial nerve indicated.

Figure 2: Simplification of the point source moving along the x-axis. The velocity of the moving point is equal to the feed rate of the drilling process.

Figure 3: Left: *In vivo* experimental setup with surgical robot (temperature measurement equipment not visible); Right: Example of 3 planned drilling trajectories with a distance of 0.5 mm in-between the edges. All 12 holes are planned accordingly. Drilled holes function in many cases as measurement hole for the next drilling. In this case is the green trajectory is the first measurement hole for the first drilling trajectory (closer blue trajectory).

Figure 4: Left: Measurement setup with thermocouple and drill bit advancing into the bone; Right: Post-op μCT of two neighboring drilled holes.

Figure 5:Regression of calculated and measured maximal temperatures with calibration of the model using all measurement data. Linear regression line and y=x line (dashed) are shown.

Figure 6: Comparison of calculated and measured temperatures over time for a distance of 3 mm. Root meant square errors (RMSE) and errors at maximal temperature (ERMT) of measured and predicted temperatures are shown. The green line shows the density profile of the drilling trajectory. The rise of the density profile above 0 HU denotes the start of the drilling process, while the drop to 0 HU shows the end of the drilled trajectory. All negative HU values were set to zero. The blue point shows at which depth (time) the drilled trajectory reaches (would reach) the depth of the measurement hole.

Figure 7: Calculated temperature curves for measurement position and theoretical minimum distance to facial nerve (1.4 mm distance to axis represents distance of 0.5 mm to the edge of the drilled hole). Maximal reached temperatures and cumulative equivalent minutes at 43°C are shown.